Supporting Information

Defective NiCo-Pentlandite/Black Phosphorus Heterostructure for Efficient Water Splitting Electrocatalysis

Hang Liu,[a,‡] *Yahui Tian,*[b,‡] *Syama Lenus,*[a] *Xin Zhao,*[a] *Zhengfei Dai,*[a] *and Tingting Liang* [a,c*]

[a] State Key Laboratory for Mechanical Behavior of Materials, Xi'an Jiaotong University, Xi'an 710049, China

[b] Institute of Physical Science and Information Technology, Anhui University, Hefei 230601, China

[c] School of Materials Science and Engineering, Henan University of Science and Technology, Luoyang 471023, China

‡ These authors contribute equally to this work.

*Corresponding author: liangtingting@haust.edu.cn

S1. Synthesis of the Ni-Co_9S_8/BP heterostructure

1. Preparation of the Ni-$Co(OH)_2$/BP heterostructure.

All reagents of analytical grade were used without further purification. The BP lamellae were prepared through exfoliation method, based on our previous report.[1] To prepare Ni-$Co(OH)_2$/BP, initially two precursors $CoSO_4 \cdot 7H_2O$ (2.811g) and $NiSO_4 \cdot 6H_2O$ (2.6285g) were dissolved together into 30 mL of deionized (DI) water to make the homogenous mixture. 100 mg BP lamellae were dispersed into 20 mL DI water, and the solution was then added into the mixture. Afterward, 5 mL of $NH_3 \cdot H_2O$ was inserted dropwise at a stirring rate of 1000 r/min for 5 min at room temperature. To remove the surfactant and residual ions on the surface, the suspension was clearly washed with absolute ethanol and water for at least 4 times. Ni-$Co(OH)_2$/BP was finally obtained by annealing at 60 °C under vacuum condition for 6 h. Besides, $Co(OH)_2$/BP was also synthesized via the above-mentioned recipe except the introduction of $NiSO_4 \cdot 6H_2O$.

2. Preparation of the Ni-Co_9S_8/BP heterostructure.

Sulfur powder and Ni-$Co(OH)_2$/BP powder were prepared as precursors and kept at two separate positions in a porcelain boat with sulfur powder at the upstream side of the tube furnace. The samples were annealed under Ar atmosphere at 350 °C for 2 h with a ramping rate of 2 °C/min. The final product Ni-Co_9S_8/BP was obtained in black color after naturally cooling to room temperature. In a parallel experiment, Co_9S_8/BP was synthesized using $Co(OH)_2$/BP powder under the identical conditions. For comparison, Co_9S_8 and Ni-Co_9S_8 samples were also prepared without BP participation.

S2. Characterizations

The morphological and structural analysis of the materials were carried out using the field emission scanning electron microscope (FESEM, FEI Verios 460) and transmission electron microscope (TEM, JEM-2100F) with the energy dispersive X-ray spectrometer (EDX). X-ray diffraction (XRD) measurements were done to investigate the crystalline structures of the synthesized samples with λ of 1.5405 Å on PANalytical X'Pert Pro. Furthermore, X-ray photoelectron spectroscopy (XPS, Thermo Fisher Scientific ESCALAB Xi+) was employed to study the surface states of the samples. Bruker ELEXSYS electron paramagnetic resonance (EPR) system was used to detect the vacancies in the samples, which was operated with the frequency of 9.86 GHz and the modulation frequency of 100 KHz at room temperature. Brunauer–Emmett–Teller (BET) surface area was detected by ASAP 2020 Plus HD88 using N_2 for degassing process. The bonding states of Co elements in the samples were measured by synchrotron radiation source. Rh K-edge XAFS analyses were performed with Si (111) crystal monochromators at the BL14W Beam line at the Shanghai Synchrotron Radiation Facility (SSRF) (Shanghai, China). Before the analysis at the beamline, samples were placed into aluminum sample holders and sealed using Kapton tape film. The XAFS spectra were recorded at room temperature using a 4-channel Silicon Drift Detector (SDD) Bruker 5040. Rh K-edge extended X-ray absorption fine structure (EXAFS) spectra were recorded in transmission/fluorescence mode. Negligible changes in the line-shape and peak position of Rh K-edge XANES spectra were observed between two scans taken for a specific sample. The XAFS spectra of these standard samples were recorded in transmission mode. The spectra were processed and analyzed by the software codes Athena. Artemis is used for Fourier transform fitting. For the wavelet transform analysis, the $\chi(k)^3$ derived from Athena was input into the Hama Fortran code, the R was set to 0-6 Å.

S3. Electrochemical measurements.

The BP, $Co(OH)_2$/BP, Ni-$Co(OH)_2$/BP, Co_9S_8, Co_9S_8/BP, Ni-Co_9S_8, Ni-Co_9S_8/BP were used as working electrodes, a Hg/HgO as a reference electrode and a graphite rod as a counter electrode in 1 M KOH or 0.5 M H_2SO_4 solution. Catalysts (4 mg) materials and acetylene carbon black (1 mg) were mixed and placed into a glass bottle, and then the add ethanol (0.9 mL), ultrapure water (0.08 mL) and 5 wt% Nafion (0.02 mL) into the bottle, through sonication for about 2 h. Afterward, the catalytic ink (5 µL) was dripped on a glass carbon (GC, 3 mm) work electrode, forming a thin film on GC surface. HER and OER performances of the samples were detected in acid solution (0.5 M H_2SO_4) and alkaline electrolyte (1M KOH) using Autolab PGSTAT204 workstation with a standard three-electrode system, as demonstrated in our previous work.[1,2] Linear sweep voltammetry (LSV) curves were tested at the potential range from 1.2 to 1.8 V (vs RHE) for OER and the potential range from −0.5 to 0.1 V (vs RHE) for HER with a scan speed of 5 mV s^{-1}, respectively. Electrochemical impedance spectroscopy (EIS) was detected to study the charge transfer resistance (R_{ct}), operating from 100 kHz to 0.1 Hz with 5 mV amplitude. At last, a two-electrode setup with two working electrodes was assembled for EWS in 1 M KOH solution within the range of 1-1.8 V (vs RHE) at a scan speed of 5 mV s^{-1}.

Figure S1 Hang Liu *et al.*

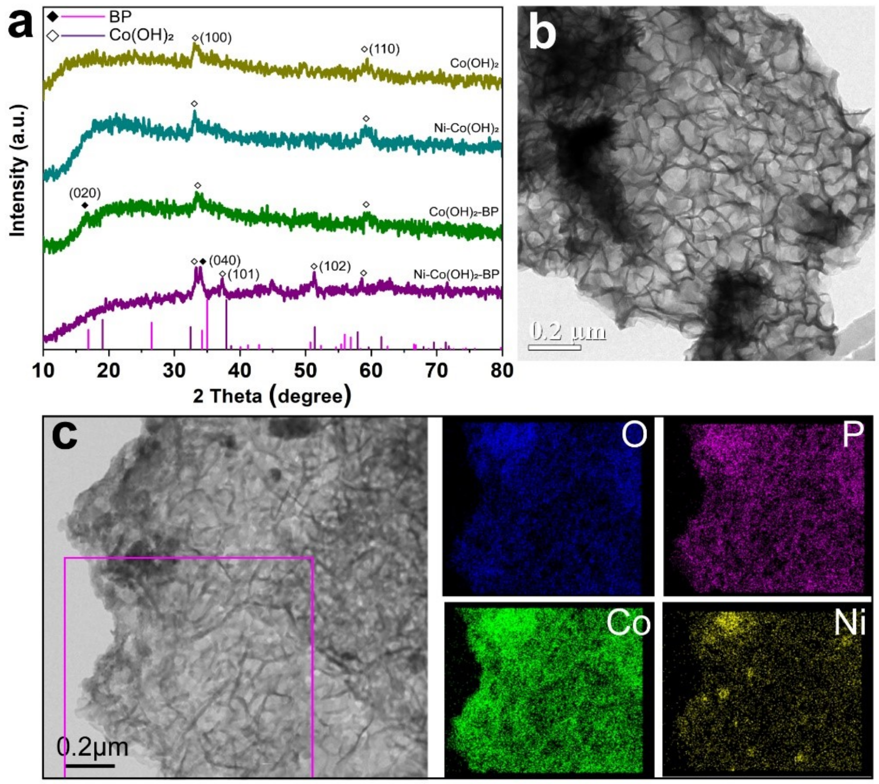

Fig. S1 (a) XRD patterns of $Co(OH)_2$, Ni- $Co(OH)_2$, $Co(OH)_2$-BP and Ni- $Co(OH)_2$/BP, respectively. (b) TEM images and (c) elemental mapping images of Ni- $Co(OH)_2$/BP.

Figure S2 Hang Liu *et al.*

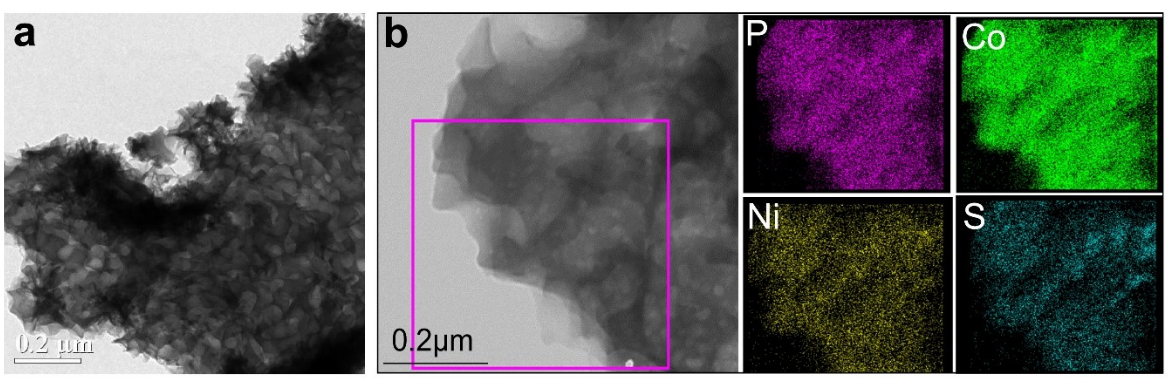

Fig. S2 (a) TEM images and (b) elemental mapping images of Ni-Co_9S_8/BP.

Figure S3 Hang Liu *et al.*

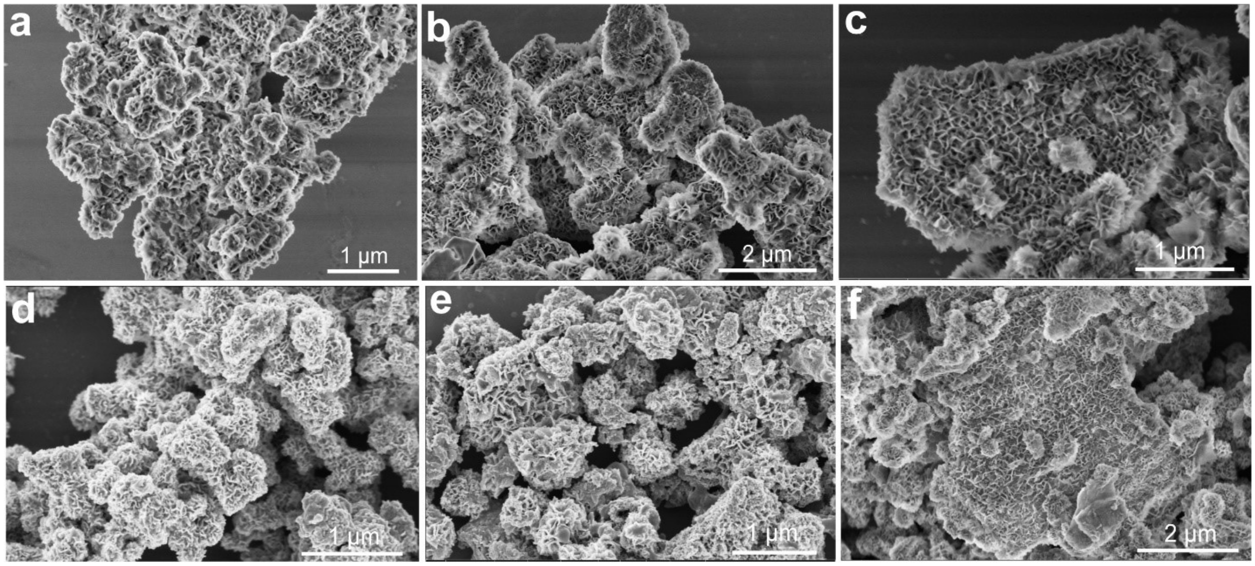

Fig. S3. SEM images of (a) $Co(OH)_2$, (b) Ni-$Co(OH)_2$, (c) $Co(OH)_2$/BP, (d) Co_9S_8, (e) Ni-Co_9S_8, and (f) Co_9S_8/BP, respectively.

Figure S4 Hang Liu *et al.*

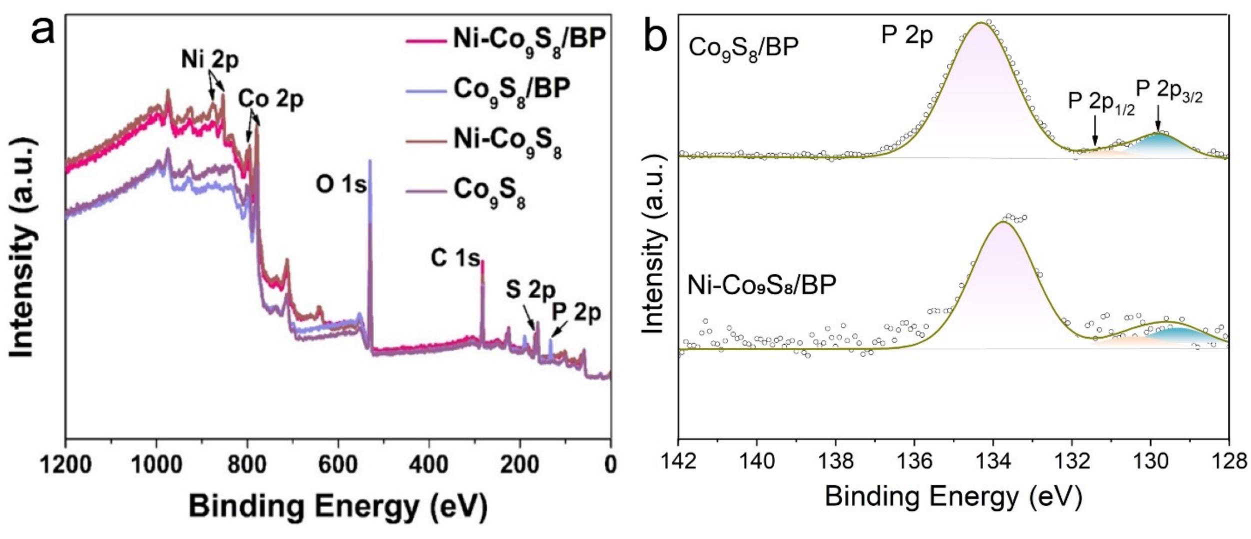

Fig. S4. (a) XPS survey of Co_9S_8, Co_9S_8/BP, Ni-Co_9S_8, and Ni-Co_9S_8/BP, respectively. (b) High-resolution P 2p XPS spectra of Co_9S_8/BP and Ni-Co_9S_8/BP, respectively.

Figure S5 Hang Liu *et al.*

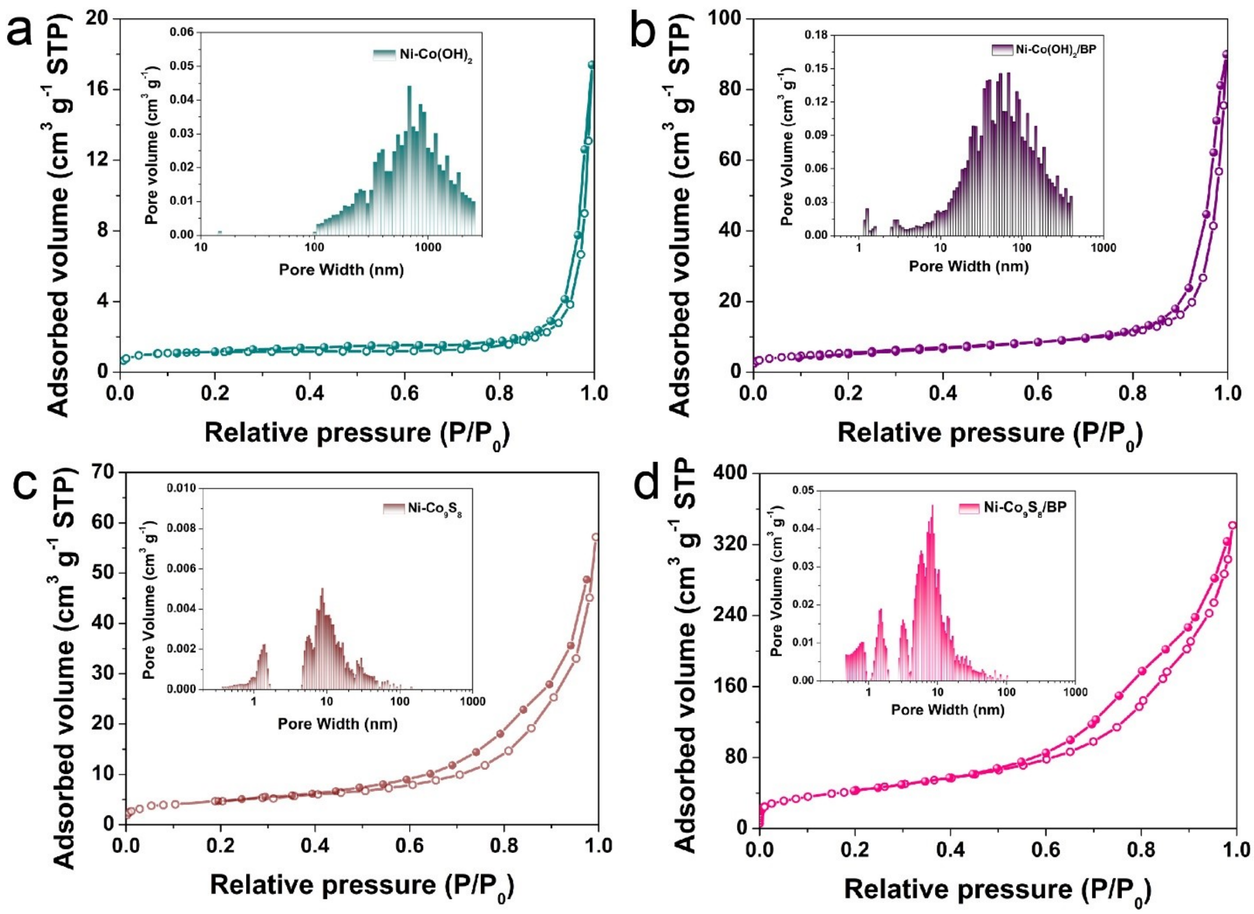

Fig. S5 N_2 adsorption/desorption curves and pore width distribution of (a) Ni-$Co(OH)_2$, (b) Ni-$Co(OH)_2$/BP, (c) Ni-Co_9S_8 and (d) Ni-Co_9S_8/BP, respectively.

Figure S6 Hang Liu *et al.*

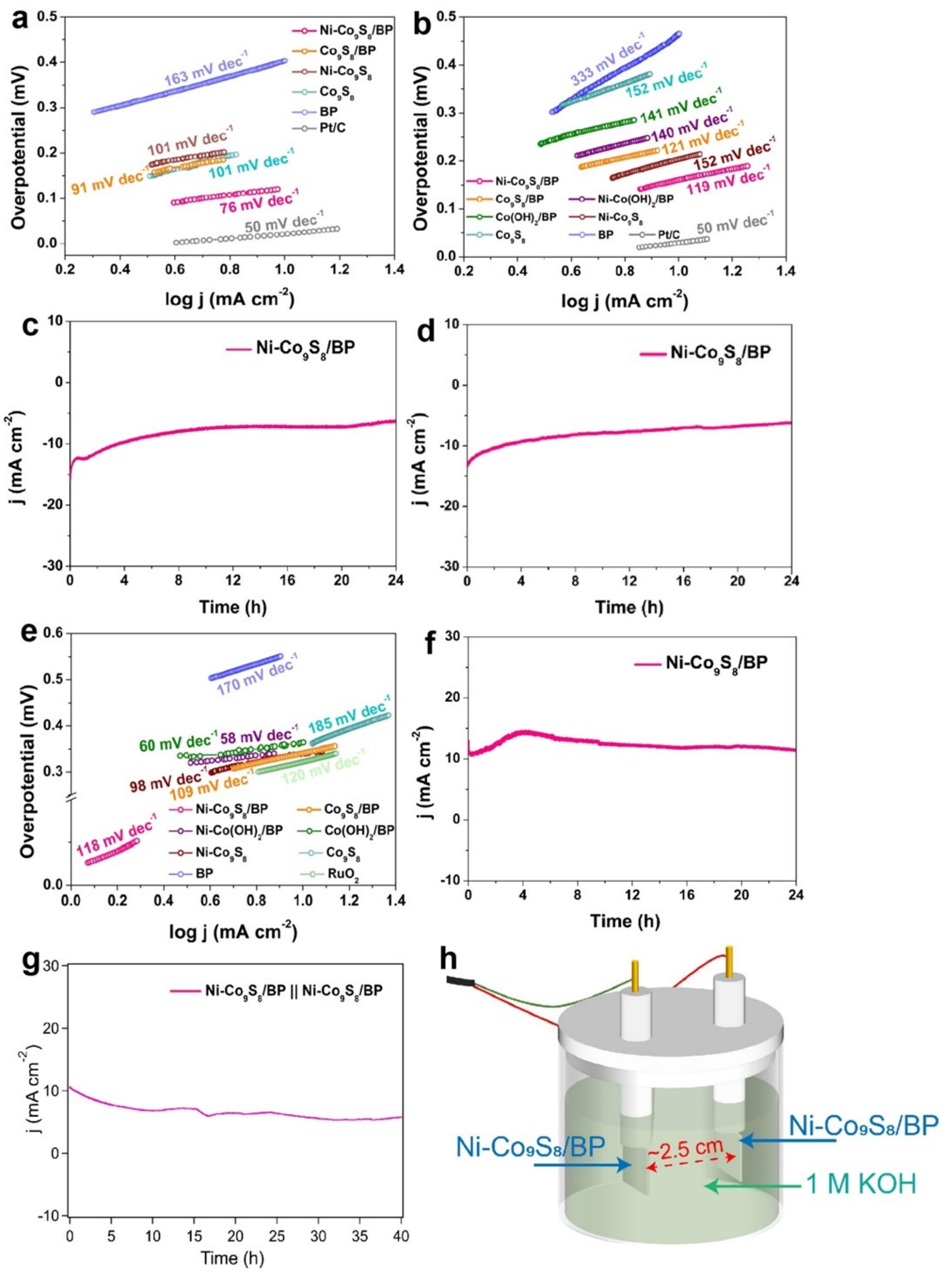

Fig. S6 Tafel plots of catalysts for HER in (a) 0.5 M H_2SO_4 and (b) in 1M KOH. Chronopotentiometry test for HER in (c) 0.5 M H_2SO_4 and (d) 1M KOH. (e) Tafel plots of catalysts for OER. (f) Chronopotentiometry test for OER in 1M KOH. (g) Chronopotentiometry test of overall water splitting based on the Ni-Co_9S_8/BP||Ni-Co_9S_8/BP couple. (h) Schematic of the two-electrode configuration.

Figure S7 Hang Liu *et al.*

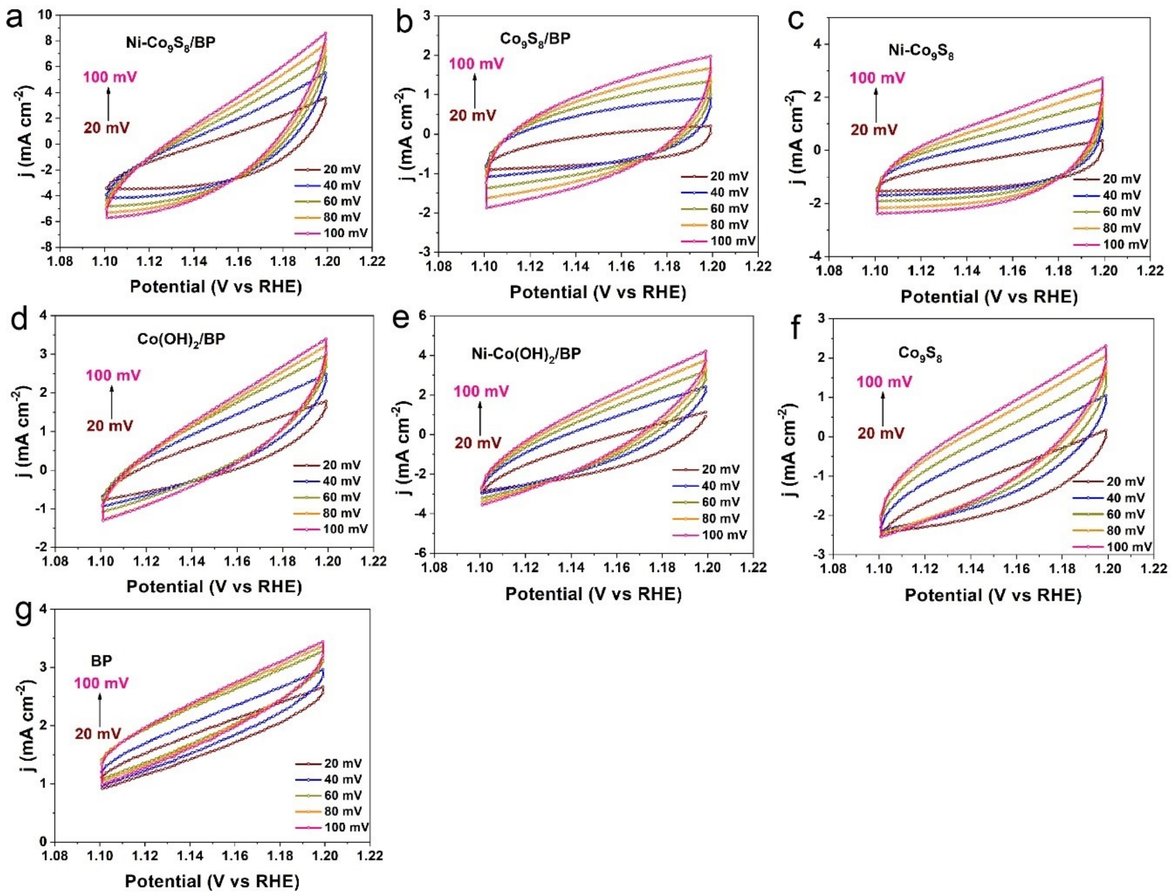

Fig. S7 CV curves with different scan rates of catalysts. (a) Ni-Co_9S_8/BP, (b) Co_9S_8/BP, (c) Ni-Co_9S_8, (d) $Co(OH)_2$/BP, (e) Ni-$Co(OH)_2$/BP, (f) Co_9S_8 and (g) BP, respectively.

Figure S8 Hang Liu *et al.*

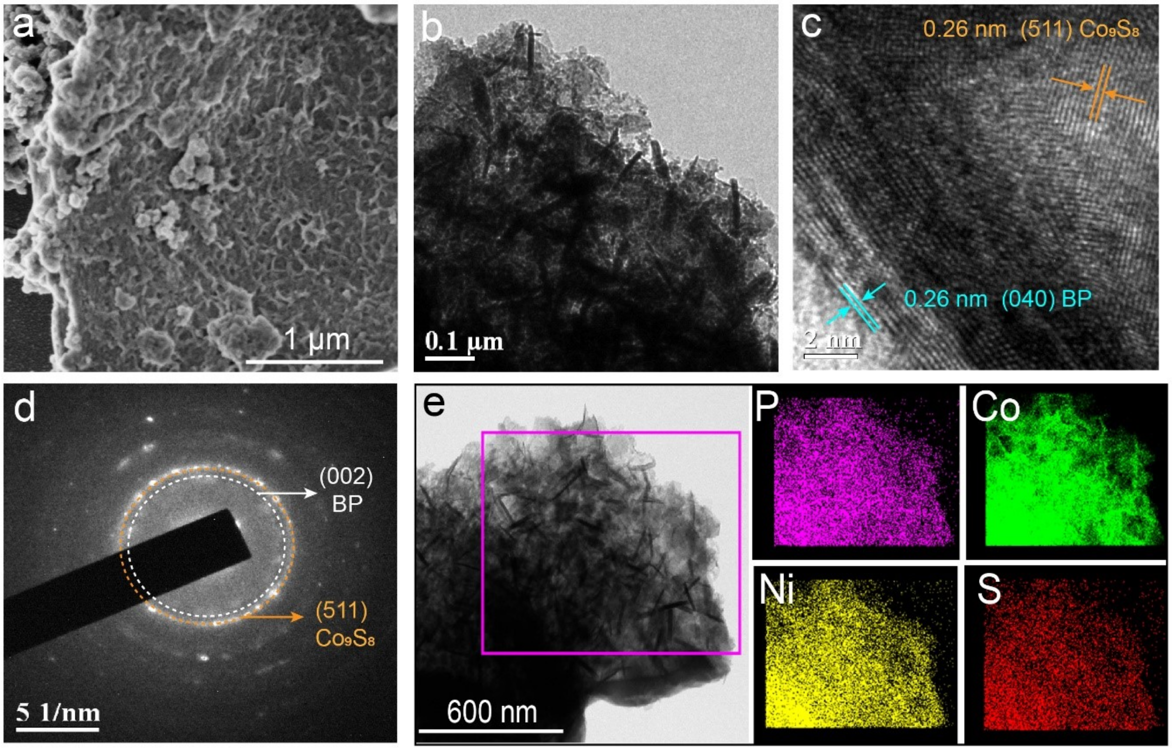

Fig. S8 Morphologies of Ni-Co_9S_8/BP after OER stability test. (a) SEM image, (b) TEM image, (c) HRTEM image, (d) SAED image, and (e) EDX mappings, respectively.

Table S1. Comparison of the HER performance of Ni-Co_9S_8/BP with those of the relevant catalysts in 0.5 M H_2SO_4 and 1M KOH.

Catalysts	Tafel Slope (mV dec^{-1})	Overpotential (η_{10}, mV)	Electrolyte	Ref.
Co_9S_8 HMs-140/C	108	250	0.1 M KOH	3
Co_9S_8@NPC-10	101.8	261	1 M KOH	4
Co_9S_8@NC	154.1	343	1 M KOH	4
EBP@NG	109	210	1 M KOH	5
CoP/EEBP	158	291	1 M KOH	6
BP	333	464	1 M KOH	6
Co_9S_8-NSC@Mo_2C	106.4	121	1 M PBS	7
Co_9S_8/CNFs	83	165	0.5 M H_2SO_4	8
$(Co\text{-}CoS_2)_x$@ Co_9S_8	51.0	460	0.5 M H_2SO_4	9
$MoSe_2$-BP	97	380	0.5 M H_2SO_4	10
Ni_2P@BP	38.6	107	0.5 M H_2SO_4	11
Ni- Co_9S_8/BP	76	121	0.5 M H_2SO_4	This work
	119	160	1 M KOH	

Hollow microspheres (HM)

N, S-co-doped carbon (NSC)

N, P doped porous carbon (NPC)

N-doped porous carbon (NC)

Carbon nanofibers (CNF)

Black phosphorus (BP)

Few-layered exfoliated black phosphorus (EBP)

Electrochemical exfoliated black phosphorus (EEBP)

Nitrogen Doped Graphene (NG)
Phosphate buffer solution (PBS)

Table S2. Comparison of the OER performance of Ni-Co_9S_8/BP with those of the relevant catalysts in 1M KOH.

Catalysts	Tafel Slope (mV dec^{-1})	Overpotential (mV)	Electrolyte	Ref
Co_9S_8-NSC@Mo_2C	59.7	293	1 M KOH	7
N-Co_9S_8/G	82.7	409	0.1 M KOH	12
Co_9S_8@NOSC	68	340	1 M KOH	13
Co_9S_8 nanoarrays	56	265	1 M KOH	14
Co_9S_8/N, S-CNTs	106	379	0.1 M KOH	15
Co_9S_8@NSC	217	549	0.1 M KOH	16
Co_9S_8/N, S-DLCTs	95	367	0.1 M KOH	17
Co/Co_9S_8 NPs	265	550	0.1 M KOH	18
CoS-RGO	71	350	1 M KOH	19
$Co(OH)_2$/BP	57	276	1 M KOH	20
Ni-Co_9S_8/BP	118	258	1 M KOH	This work

Graphene (G)
Hollow microspheres (HM)
N, S-co-doped carbon (NSC)
N-, O-, and S-tridoped carbon (NOSC)
Carbon nanotubes (CNT)
(N, S)-Doped Double-Layered Carbon Tubes (DLCT)
Few-layer graphene (RGO)
Black phosphorus (BP)

Table S3. Comparison of the overall water splitting performance of Ni-Co_9S_8/BP with those of the relevant catalysts in 1M KOH.

Catalysts	η_{HER}@10 mA cm^{-2} (mV)	η_{OER}@10 mA cm^{-2} (mV)	Voltage at η_{10} (V)	Electrolyte	Ref.
CoS-RGO	118	350	1.77	1 M KOH	19
Mo-Co_9S_8@C	98	370	1.68	0.5 M H_2SO_4	21
MoS_2/Co_9S_8/Ni_3S_2/Ni	117	405	1.88	1.0 M PBS	22
CoS_2 NTA/CC	193	276	1.67	1 M KOH	23
Co_9S_8@MoS_2	143	340	1.67	1 M KOH	24
Co_9S_8-$CoSe_2$	150	340	1.66	1 M KOH	25
BP QDs/MXene	190	360	1.78	1 M KOH	26
Co-Fe oxyphosphide	180	280	1.69	1 M KOH	27
Ni2.3%-CoS_2/CC	231 η_{100}	370 η_{100}	1.66	1 M KOH	28
Ni- Co_9S_8/BP ‖ Ni- Co_9S_8/BP	160	258	1.65	1 M KOH	**This work**

Few-layer graphene (RGO)

Electrochemical exfoliated black phosphorus (EEBP)

Quantum Dot (QD)

Black phosphorus (BP)

Nanotube arrays (NTA)

Carbon Cloth (CC)

Phosphate buffer solution (PBS)

References

1 T. T. Liang, S. Lenus, Y. D. Liu, Y. Chen, T. Sakthivel, F. Y. Chen, F. Ma and Z. F. Dai, *Energy Environ. Mater.*, 2023, 6, e12332.

2 W. F. Zhai, Y. Chen, Y. D. Liu, T. Sakthivel, Y. Y. Ma, S. W. Guo, Y. Q. Qu and Z. F. Dai, *Adv. Funct. Mater.*, 2023, 33, 2301565.

3 Y. T. Zhang, S. J. Chao, X. B. Wang, H. J. Han, Z. Y. Bai and L. Yang, *Electrochim. Acta*, 2017, 246, 380-390.

4 R. R. Liu, H. M. Zhang, X. Zhang, T. X. Wu, H. J. Zhao and G. Z. Wang, *RSC Adv.*, 2017, 7, 19181-19188.

5 Z. K. Yuan, J. Li, M. J. Yang, Z. S. Fang, J. H. Jian, D. S. Yu, X. D. Chen and L. M. Dai, *J. Am. Chem. Soc.,* 2019, 141, 4972-4979.

6 T. T. Liang, Y. D. Liu, P. F. Zhang, C. T. Liu, F. Ma, Q. Y. Yan and Z. F. Dai, *Chem. Eng. J.*, 2020, 395, 124976.

7 X. H. Luo, Q. L. Zhou, S. Du, J. Li, J. W. Zhong, X. L. Deng and Y. L. Liu, *ACS Appl. Mater. Interfaces*, 2018, 10, 22291-22302.

8 L. Gu, H. Zhu, D. N. Yu, S. G. Zhang, J. W. Chen, J. Wang, M. Wan, M. Zhang and M. L. Du, *Part. Part. Syst. Char.*, 2017, 34, 1700189.

9 X. W. Zhang, Y. Y. Liu, J. Gao, G. S. Han, M. F. Hu, X. L. Wu, H. Q. Cao, X. Y. Wang and B. J. Li, *J. Mater. Chem. A*, 2018, 6, 7977-7987.

10 W. Li, D. N. Liu, N. Yang, J. H. Wang, M. Y. Huang, L. L. Liu, X. Peng, G. M. Wang, X. -F. Yu, P. K. Chu, *Appl. Surf. Sci.*, 2019, 467, 328-334.

11 Z. Z. Luo, Y. Zhang, C. H. Zhang, H. T. Tan, Z. Li, A. Abutaha, X. L. Wu, Q. H. Xiong, K. A. Khor, K. Hippalgaonkar, J. W. Xu, H. H. Hng and Q. Y. Yan, *Adv. Energy Mater.*, 2017, 7, 1601285.

12 S. Dou, L. Tao, J. Huo, S. Y. Wang and L. M. Dai, *Energ. Environ. Sci*., 2016, 9, 1320-1326.

13 S. C. Huang, Y. Y. Meng, S. M. He, A. Goswami, Q. L. Wu, J. H. Li, S. F. Tong, T. Asefa and M. M. Wu, *Adv. Funct. Mater.*, 2017, 27, 1606585.

14 H. X. Zhang, J. Y. Wang, Q. L. Cheng, P. Saha, H. Jiang, *Green Energy Environ.*, 2020, 5, 492-498.

15 L. L. Chen, W. X. Yang, X. J. Liu, L. Long, D. D. Li and J. B. Jia, *Nanotechnology*, 2018, 30, 075402.

16 S. M. Alshehri, J. Ahmed, A. Khan, M. Naushad and T. Ahamad, *ChemElectroChem*, 2018, 5, 355-361.

17 C. C. Hu, J. Liu, J. Wang, W. X. She, J. W. Xiao, J. B. Xi, Z. W. Bai and S. Wang, *ACS Appl. Mater. Interfaces*, 2018, 10, 33124-33134.

18 H. B. Zhang, F. Q. Niu, S. Y. Li, Y. H. Yin, H. Y. Dong, H. Y. Yue, Z. X. Cao and S. T. Yang, *New J. Chem.*, 2020, 44, 9522-9529.

19 Y. N. Chen, S. M. Xu, S. Z. Zhu, R. J. Jacob, G. Pastel, Y. B. Wang, Y. J. Li, J. Q. Dai, F. J. Chen, H. Xie, B. Y. Liu, Y. G. Yao, L. G. Salamanca-Riba, M. R. Zachariah, T. Li and L. B. Hu, *Nano Res.* 2019, 12, 2259-2267.

20 Y. J. Li, C. G. Liao, K. W. Tang, N. Zhang, W. H. Qi, H. P. Xie, J. He, K. Yin, Y. L. Gao and C. D. Wang, *Electrochim. Acta*, 2019, 297, 40-45.

21 L. G. Wang, X. X. Duan, X. J. Liu, J. Gu, R. Si, Y. Qiu, Y. M. Qiu, D. E. Shi, F. H. Chen, X. M. Sun, J. H. Lin and J. L. Sun, *Adv. Energy Mater.*, 2020, 10, 1903137.

22 Y. Yang, H. Q. Yao, Z. H. Yu, S. M. Islam, H. Y. He, M. W. Yuan, Y. H. Yue, K. Xu, W. C. Hao, G. B. Sun, H. F. Li, S. L. Ma, P. Zapol and M. G. Kanatzidiz, *J. Am. Chem, Soc.*, 2019, 141, 10417-10430.

23 C. Guan, X. M. Liu, A. M. Elshahawy, H. Zhang, H. J. Wu, S. J. Pennycook and J. Wang, *Nanoscale Horiz*., 2017, 2, 342-348.

24 J. M. Bai, T. Meng, D. L. Guo, S. G. Wang, B. G. Mao and M. H. Cao, *ACS Appl. Mater. Interfaces*, 2018, 10, 1678-1689.

25 S. Chakrabartty, S. Karmakar and C. R. Raj, *ACS Appl. Nano Mater.*, 2020, 3, 11326-11334.

26 X. D. Zhu, Y. Xie, Y. T. Liu, *J. Mater. Chem. A*, 2018, 6, 21255-21260.

27 P. Zhang, X. F. Lu, J. W. Nai, S. Q. Zang and D. Lou, *Adv. Sci*., 2019, 6, 1900576.

28 W. Z. Fang, D. N. Liu, Q. Lu, X. P. Sun and A. M. Asiri, *Electrochem. Commun.*, 2016, 63, 60-64.